Talanta 85 (2011) 2605–2613

Contents lists available at ScienceDirect

Talanta

journal homepage: www.elsevier.com/locate/talanta

Optimisation of ICP-MS collision/reaction cell conditions for the determination of elements likely to be interfered (V, Cr, Fe, Co, Ni, As and Se) in foodstuffs

Ali Kadar, Laurent Noël, Rachida Chekri, Christelle Vastel, Sandrine Millour, Thierry Guérin*

Anses, agence nationale de sécurité sanitaire de l'alimentation, de l'environnement et du travail, Laboratoire de Sécurité des Aliments de Maisons-Alfort, unité des Contaminants Inorganiques et Minéraux de l'Environnement, 23, Avenue du Général de Gaulle, F-94706 Maisons-Alfort, France

ARTICLE INFO

Article history:
Received 19 April 2011
Received in revised form 8 August 2011
Accepted 11 August 2011
Available online 19 August 2011

Keywords:
Inductively coupled plasma mass spectrometry
Collision cell
Experimental design
Interference
Method validation
Foodstuffs

ABSTRACT

A strategy for the accurate determination in foodstuffs of seven elements liable to be interfered with (V, Cr, Fe, Co, Ni, As and Se), was successfully applied. Firstly, to reduce spectroscopic interferences, four influential factors (hexapole and quadrupole bias, helium and hydrogen flows) of the collision/reaction cell device were optimised through the experimental design methodology. Secondly, non-spectroscopic interferences, which may severely disturb the analysis of matrices containing large amounts of non-target elements, were significantly reduced by a limited decrease in the flow rate of the optimum initial nebuliser rather than with a specific time-consuming dilution. Finally, the optimised multi-element method was subjected to a full validation that demonstrated its acceptable analytical performance.

1. Introduction

The amount of major and trace elements ingested by humans is directly related to dietary habits and the concentrations of these elements in foodstuffs. Deficiencies, excesses, or imbalances in the supply of inorganic elements from dietary sources can have a significant deleterious influence on human health [1]. It is thus important to determine precisely their levels in foodstuffs to better evaluate the nutritional as well as toxicological value of the food items [2].

Over the last few decades, different atomic spectrometry techniques such as flame atomic absorption spectrometry (FAAS) [3–6], electro-thermal atomic absorption spectroscopy (ETAAS) [7–10], inductively coupled plasma atomic emission spectroscopy (ICP-AES) [11–13] and inductively coupled plasma mass spectrometry (ICP-MS) [14–18] have been used to monitor major and trace elements. Among these techniques, ICP-MS has been gaining in popularity over the last few years because it offers the possibility of multi-element analysis through isotope monitoring with high sensitivity and short-time analysis with a large dynamic range [2]. Nevertheless, like any sensitive analytical technique, ICP-MS still has some limitations, such as spectroscopic and non-spectroscopic interferences. These interferences can be due to the overlapping isotopes of concomitant elements, either the presence in the sample solution or the formation in the plasma of polyatomic ions. Indeed, the analysis of vanadium (V), chromium (Cr), iron (Fe), cobalt (Co), nickel (Ni), arsenic (As) and selenium (Se) may be difficult in such complex matrices as foods are. Specifically, $^{51}V^{+}$ is mainly interfered with by $^{34}S^{16}O^{1}H^{+}$ and $^{35}Cl^{16}O^{+}$, $^{52}Cr^{+}$ is interfered with by $^{40}Ar^{12}C^{+}$ and $^{35}Cl^{16}O^{1}H^{+}$, $^{56}Fe^{+}$ is interfered with by $^{40}Ar^{16}O^{+}$ and $^{40}Ca^{16}O^{+}$, $^{59}Co^{+}$ is interfered with by $^{43}Ca^{16}O^{+}$ and $^{42}Ca^{16}O^{1}H^{+}$, $^{60}Ni^{+}$ is interfered with by $^{44}Ca^{16}O^{+}$ and $^{43}Ca^{16}O^{1}H^{+}$, $^{75}As^{+}$ is interfered with by $^{40}Ar^{35}Cl^{+}$ and $^{40}Ca^{35}Cl^{+}$, $^{80}Se^{+}$ is interfered with by $^{40}Ar_2{}^{+}$. The choice of an alternative isotope with lower natural abundance, and the use of correction equations or high-resolution instruments can sometimes reduce or eliminate the interference. On the other hand, collision/reaction cell technology, which has been comprehensively reviewed by Tanner et al. [19], offers new possibilities for element determination by ICP-MS. Indeed, it has proved to be an effective technique for alleviating spectroscopic interferences [20–29]. D'Ilio et al. demonstrated the satisfactory application of ICP-CCT-MS for the analysis of As and Cr in milk [28]. Bednar successfully optimised an ICP-CCT-MS instrument with oxygen as the reagent gas for indirect measurement of V [27]. Finally, our previous studies demonstrated on a first collision cell generation the benefit of using ICP-CCT-MS for the analysis of Cr, Fe and Se [22], although they also established the persistence and/or generation of interferences depending on the sample matrix components for the analysis of As, notably for the determination of low arsenic concentrations in dairy products or crab meat [26].

* Corresponding author. Tel.: +33 1 49772711.
E-mail address: thierry.guerin@anses.fr (T. Guérin).

0039-9140/$ – see front matter © 2011 Elsevier B.V. All rights reserved.
doi:10.1016/j.talanta.2011.08.027

The aim of the present work was to develop and validate a strategy based on ICP-MS with the use of a third collision cell generation for the simultaneous determination in foodstuffs of seven elements liable to be interfered with (V, Cr, Fe, Co, Ni, As, Se). In order to alleviate spectroscopic interferences, the CCT settings were, in order to reduce the number of analyses, statistically optimised through the experimental design methodology. In addition, since CCT does not act on non-spectroscopic effects, the efficiency of their attenuation was compared between different nebuliser flow rates and different dilutions of the same synthetic interfering solutions. Finally, the optimised method underwent validation in accordance with French and European standards [30–32].

2. Experimental

2.1. Reagents and materials

All solutions were prepared with analytical reagent-grade chemicals and ultrapure water (18 MΩ cm) generated by purifying distilled water with the Milli-Q^{TM} PLUS system connected to an Elix 5 pre-system (Millipore S.A., St Quentin en Yvelines, France).

Suprapur HNO_3 (67%, v/v) and HCl (30%, v/v) were purchased from VWR (Fontenay-sous-Bois, France). Standard stock solutions (1000 mg L^{-1}) of vanadium (V), chromium (Cr), iron (Fe), cobalt (Co), nickel (Ni), arsenic (As), selenium (Se), calcium (Ca), magnesium (Mg), potassium (K), sodium (Na), germanium (Ge), copper (Cu), manganese (Mn), zinc (Zn), bromine (Br) and indium (In) were purchased from Analytika (Prague, Czech Republic). Multi-element Standard Solution (10 mg L^{-1}) (Merck, Darmstadt, Germany) was used to prepare a tuning solution containing several elements such as In, uranium (U), barium (Ba) and lithium (Li), capable of covering a wide range of masses. All standards were prepared daily in 6% (v/v) HNO_3 or in 2% (v/v) HCl. Ultrapure carrier grade collision gases (He and H_2, 99.9995% pure) were purchased from Air Liquide (Paris, France). Certified Reference Materials (CRMs) NRC TORT 2 (lobster hepatopancreas) from the National Research Council of Canada (Ottawa, Ontario, Canada), IAEA 407 (fish tissue) from the International Atomic Energy Agency (Vienna, Austria), BCR 278R (mussel tissue) from the Community Bureau of Reference and NIST 1573a (tomato leaves) from the National Institute of Science and Technology (Gaithersburg, MD, USA) were all supplied by LGC Standards (Molsheim, France). Round-Robin test R 761 (milk powder), a reference material from an external proficiency testing scheme organised by the Central Science Laboratory-Food Analysis Performance Assessment Scheme (CSL-FAPAS, Sand Hutton, United Kingdom) was also used. These reference materials were used as provided, without further grinding.

2.2. Sample digestion procedure

Sample digestion was carried out using the Multiwave 3000 microwave digestion system (Anton-Paar, Courtaboeuf, France), equipped with a rotor for 8 type X sample vessels (80 mL quartz tubes, operating pressure 80 bars). Before use, quartz vessels were decontaminated in a bath of 10% HNO_3 (67%, v/v), then rinsed with ultrapure water and dried in a 40 °C oven. 0.2–0.6 g (wet mass) of samples were weighed precisely into the quartz vessels and wet-oxidised with 3 mL ultrapure grade HNO_3 (67%, v/v) and 3 mL ultrapure water. The digestion program was optimised as described previously [15]. After cooling at room temperature, sample solutions were quantitatively transferred into 50 mL polyethylene flasks and prepared under the same conditions as the calibration standards. Before final dilution, 200 μL of internal standard solution of In was added to reach the final concentration of 1 mg L^{-1}.

Table 1
ICP-MS instrumental parameters.

Plasma conditions (adjusted daily)	
RF power	1350 W
Plasma argon flow rate	15.0 L min^{-1}
Nebuliser argon flow rate	0.7–1.0 L min^{-1}
Auxiliary argon flow rate	0.5–1.0 L min^{-1}
Sampling and Skimmer cones	Nickel
Mass spectrometer settings	
Mass range	7–208 amu
Acquisition mode	Peak jumping
Number of replicates	3
Number of channels	500
Number of channels per peak	3
Dwell time (per isotope)	20 ms
Number of sweeps	500
Total acquisition time	60 s
Isotopes monitored in standard mode	^{51}V, ^{52}Cr, ^{54}Fe, ^{59}Co, ^{60}Ni, ^{75}As, ^{82}Se
Isotopes monitored in CCT mode	^{51}V, ^{52}Cr, ^{56}Fe, ^{59}Co, ^{60}Ni, ^{75}As, ^{80}Se

2.3. Instrumental determination procedure

ICP-MS measurements were performed by a Thermo Elemental X Series II instrument (Thermo Electron, Courtaboeuf, France), equipped with hexapole Collision Cell Technology (CCT). The sample solutions were pumped by peristaltic pump from tubes arranged on a CETAC ASX 500 auto-sampler (CETAC, Omaha, Nebraska, USA). Introduction into the Ar plasma was performed by a conventional pneumatic concentric nebuliser (Meinhard type A1) included in a Peltier-cooled impact bead spray chamber. Further details of the instrument settings and data acquisition parameters are given in Table 1.

Ion lens voltage, nebuliser flow, horizontal, depth and vertical positions of the torch were tuned daily by performing short-term stability tests in standard mode with a 1 μg L^{-1} tuning solution to maximise ion signals and stability while limiting the oxide levels ($CeO^+/Ce^+ < 2\%$) and doubly charged ions ($Ba^{2+}/Ba^+ < 5\%$). The collision cell was flushed with collision gases (He and/or H_2) for 10 min before a second optimisation of the torch position and ion lenses was performed in CCT mode. An internal calibration curve was plotted after the analysis of multiple reference standards, prepared at levels ranging from 0 to 50 μg L^{-1}. The calibration curve was plotted from six points, including the calibration blank (0 μg L^{-1}). In standard mode, for the measure of ^{75}As the mathematical correction equation was automatically used at *m/z* 75, based on the natural abundances of the isotopes:

$$I(^{75}As) = I(^{75}mass) - 3.127 \times [I(^{77}mass) - 0.826 \times I(^{82}Se)] \quad \text{with}$$

3.127 = abundance ^{75}ArCl/^{77}ArCl and 0.826 = abundance ^{77}Se/^{82}Se.

2.4. Optimisation of the CCT factors by central composite design (CCD)

2.4.1. CCD

After having determined the preliminary range of the net Signal-to-Background Ratio ($SBR = (X - B)/B$, where X is the gross signal of the analyte solution, B is the measurement of the interferent signal and $(X - B)$ is the net signal) dependent variables through a single-factor test, a CCD with four independent variables (X_1, He flow; X_2, H_2 flow; X_3, Hexapole bias; X_4, Quadrupole bias) was performed at five levels [33]. The ranges of these independent variables were based on the results of preliminary experiments: X_1: 0.5–5.0 mL min^{-1}; X_2: 0.5–5.0 mL min^{-1}; X_3: −9.3 to −1.3 V; X_4: −20.0 to −9.0 V. The complete design consisted of 28 experimental points (16 factorial points, 8 axial points and 4 centre points) (Table 2A).

Table 2
Values of the factors at the five levels examined (A) and experiments undertaken for the CCD (B).

(A)		He flow ($mL\,min^{-1}$)	H_2 flow ($mL\,min^{-1}$)	Hexapole bias (V)	Quadrupole bias (V)	
	Lowest	0.5	0.5	−9.3	−20.0	
	Low	1.6	1.6	−7.3	−17.3	
	Centre	2.8	2.8	−5.3	−14.6	Factor level
	High	3.9	3.9	−3.3	−11.8	
	Highest	5.0	5.0	−1.3	−9.0	
(B)	No.	X_1	X_2	X_3	X_4	$SBR^{weighted\ amount}$
	1	1.6	1.6	−7.3	−17.3	385
	2	3.9	1.6	−7.3	−17.3	522
	3	1.6	3.9	−7.3	−17.3	500
	4	3.9	3.9	−7.3	−17.3	701
	5	1.6	1.6	−3.3	−17.3	408
	6	3.9	1.6	−3.3	−17.3	536
	7	1.6	3.9	−3.3	−17.3	511
	8	3.9	3.9	−3.3	−17.3	660
	9	1.6	1.6	−7.3	−11.8	443
	10	3.9	1.6	−7.3	−11.8	726
	11	1.6	3.9	−7.3	−11.8	646
	12	3.9	3.9	−7.3	−11.8	963
	13	1.6	1.6	−3.3	−11.8	447
	14	3.9	1.6	−3.3	−11.8	629
	15	1.6	3.9	−3.3	−11.8	581
	16	3.9	3.9	−3.3	−11.8	781
	17	0.5	2.8	−5.3	−14.6	376
	18	5.0	2.8	−5.3	−14.6	731
	19	2.8	0.5	−5.3	−14.6	379
	20	2.8	5.0	−5.3	−14.6	666
	21	2.8	2.8	−9.3	−14.6	560
	22	2.8	2.8	−1.3	−14.6	548
	23	2.8	2.8	−5.3	−20.0	453
	24	2.8	2.8	−5.3	−9.0	714
	25	2.8	2.8	−5.3	−14.6	509
	26	2.8	2.8	−5.3	−14.6	508
	27	2.8	2.8	−5.3	−14.6	511
	28	2.8	2.8	−5.3	−14.6	513

2.4.2. Experimental values

A blank solution was prepared in 6% and 2% (v/v) HNO_3 and HCl, respectively, and two multi-element standard solutions were prepared in 6% and 2% (v/v) HNO_3 or in 6% (v/v) HNO_3 only at a level of 10 $\mu g\,L^{-1}$. The produced effect was evaluated by measuring the total intensity (count s^{-1}) for each element and blank solution, and by calculating the SBR.

2.4.3. Statistical analysis

The experimental data were processed using the Statgraphics Centurions XV software package (Sigma Plus, Paris, France). *p*-Values of less than 0.05 were considered to be statistically significant. In addition, the normality of the data was checked by plotting the normal probability plot (NPP) of the residuals. Data from the CCD were analysed by multiple regressions to fit the following quadratic polynomial model.

$$Y = \beta_0 + \sum_{i=1}^{4} \beta_i X_i + \sum_{i=1}^{4} \beta_{ii} X_i^2 + \sum_{i<j=2}^{4} \beta_{ij} X_i X_j$$

where Y represents the response function, β_0 the intercept and β_i, β_{ii} and β_{ij} are the linear, quadratic and interaction terms, respectively. The fitted polynomial equation is expressed as surface and contour plots in order to visualise the relationship between the response and experimental levels of each factor and to deduce the optimum conditions. The analysis of variance (ANOVA) tables were generated, and the effect and regression coefficients of individual linear, quadratic and interaction terms were determined. The regression coefficients were then used to perform a statistical calculation to generate dimensional and contour maps from the regression models.

2.5. Method validation

The method was validated by analysing different foodstuffs such as meat, fish and dairy products or vegetables. Concentrations were expressed in milligrams of elements per kg ($mg\,kg^{-1}$) of fresh material. Several parameters were taken into account and evaluated for the in-house validation of the method: range of linearity, limits of quantification (LOQ), selectivity/specificity, trueness and precision by evaluating the repeatability and the within-laboratory reproducibility. The method was validated according to the French NF EN 13804 [30], NF V 03-110 [31] and NF V 03-115 standards [32]. In the case of routine analysis, during the validation, as part of the adopted internal quality control (IQC) procedure, an analytical sequence included a reagent blank and a CRM. To check the absence of any pollution or significant drift of the instrument sensitivity, after each set of five samples run, a blank digested sample containing In internal standard at 4 $\mu g\,L^{-1}$ was analysed. A maximum drift of 10% based on the sensitivity of the last calibration standard was considered acceptable for the aim of the validation study.

3. Results and discussion

3.1. Statistical analysis and optimisation of the factors

After collecting the experimental data and validating the fitting of a second-order model separately for each element (data

Table 3
ANOVA of central composite design.

Parameter	SS	df	MS	*F*	*p*
X_1	**221,760**	**1**	**221,760**	**238.4**	**0.0000**
X_2	**138,168**	**1**	**138,168**	**148.5**	**0.0000**
X_3	**5310**	**1**	**5310**	**5.71**	**0.0327**
X_4	**95,634**	**1**	**95,634**	**102.8**	**0.0000**
X_1^2	6859	1	6859	7.37	0.0177
X_1X_2	1173	1	1173	1.26	0.2818
X_1X_3	**4865**	**1**	**4865**	**5.23**	**0.0396**
X_1X_4	**8418**	**1**	**8418**	**9.05**	**0.0101**
X_2^2	2012	1	2012	2.16	0.1651
X_2X_3	3052	1	3052	3.28	0.0932
X_2X_4	2626	1	2626	2.82	0.1167
X_3^2	**6961**	**1**	**6961**	**7.48**	**0.0170**
X_3X_4	**7525**	**1**	**7525**	**8.09**	**0.0138**
X_4^2	**14,296**	**1**	**14,296**	**15.4**	**0.0018**
Error	12,092	13	930		
Total SS	519,971	27			

SS = sum of squares, df = degree of freedom, MS = mean square, *F* = ratio, and *p* = probability level.

not shown), a weighted average of SBR responses was calculated (Table 2B). Then, by applying multiple regression analysis to these values, the response variable and the investigated variables allowed the following second-polynomial equation to be established:

$$Y = 840 + 61X_1 + 37X_2 + 18X_3 + 65X_4 + 13X_1^2 + 6X_1X_2 - 8X_1X_3 + 7X_1X_4 + 7X_2^2 - 6X_2X_3 + 4X_2X_4 + 4X_3^2 - 4X_3X_4 + 3X_4^2$$

The determination coefficient ($R^2 = 0.977$) was obtained by ANOVA of the quadratic regression model, indicating that only 2.3% of the total variations were not explained by this model. The value of the adjusted determination coefficient also confirmed that the model was highly significant (adjusted $R^2 = 0.952$). As a consequence, the model was found to be adequate for prediction within the range of experimental variables. Significant effects for interference elimination are displayed in bold in Table 3, thus the linear coefficients (X_1, X_2, X_3, X_4), the quadratic term coefficients (X_1^2, X_3^2, X_4^2) and the cross product coefficients (X_1X_3, X_1X_4, X_3X_4) were all significant.

Then, in order to allow the prediction of the SBR response within the experimentally studied range, the full regression equation was graphically represented by the three-dimensional response surface plot (Fig. 1) and two-dimensional contour plot (Fig. 2). In both figures, the SBR was obtained along with two continuous variables, while the other two variables were fixed constants.

The 3-D response surface plot, which gives the SBR response as a function of Hexapole bias, X_3 and Quadrupole bias, X_4 at fixed H_2 and He flows (X_1 and X_2 at centre values), indicated that the area of maximum SBR is located at the lowest and highest level of Hexapole and Quadrupole bias, respectively. On the other hand, the 2-D contour plot, which displays the SBR response as a function of H_2 flow, X_1 and He flow, X_2 at fixed Hexapole bias, X_3 and Quadrupole bias, X_4 (−9.0 and −13.2 V, respectively), indicated that the SBR is maximised due to high flows of at least He gas or a mixture of both He (high level) and H_2 gases. Note that to maintain reasonable sensitivity and to prevent cell pressure regulation problems, it is better to limit the total amount of gas injected. Then two areas would be suitable for maximising the SBR: on the one hand, a high H_2 value with a low He value, and on the other hand, a high He value with a low H_2 value. Besides, it should be noted that a high H_2 flow induces the production of considerable second-order spectroscopic interferences at $m/z = 80$ ($^{79}Br + {}^1H \rightarrow {}^{80}BrH$), causing a positive bias of ^{80}Se amounts [34]. Consequently, the optimised chosen values were defined as follows: He flow: 4.5 mL min^{-1}; H_2 flow: 0.5 mL min^{-1}; hexapole bias: −9.0 V; quadrupole bias: −13.2 V.

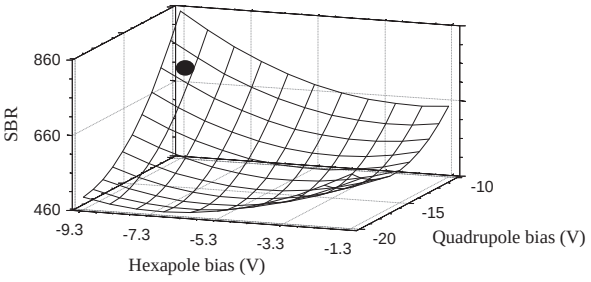

Fig. 1. Response surface plot (3-D) showing the effects of the Hexapole bias and Quadrupole bias variables at fixed He and H_2 flow values (2.75 mL min^{-1}) on the SBR response.

3.2. Evaluation of potential interferences

As previously demonstrated [22], the optimised CCT conditions led to a drastic reduction in the main argon-based interferences of the major isotopes ^{52}Cr, ^{56}Fe and ^{80}Se at mass to charge ratios (m/z): 52 ($^{40}Ar^{12}C$), 56 ($^{40}Ar^{16}O$) and 80 ($^{40}Ar^{40}Ar$). In the same way, the presence of major chloride-based first-order interferences ($^{40}Ar^{35}Cl$ on ^{75}As, $^{35}Cl^{16}O$ on ^{51}V and $^{35}Cl^{16}O^1H$ on ^{52}Cr) was evaluated. Secondly, the optimised setup conditions for the potentials between the quadrupole mass analyser and the hexapole cell constitute non-kinetic energy discrimination (KED) conditions ($X_4 - X_3 < 0$). KED values were described as being efficient at reducing the transmission to the mass analyser of new in-cell formed interferences [37]. However, several authors did not use KED in their determinations as optimum operational conditions [20,38–40] depending in particular on the cell gases used and the m/z of the element. In these conditions, the generation of second-order polyatomic ions during the analysis of As was demonstrated [26]. On the other hand, Fraser and Beauchemin [35] described the probable occurrence of signal elimination or enhancement depending on the sample matrix composition. So, to estimate the presence or absence of both spectroscopic and non-spectroscopic interferences, different mimetic samples containing high amounts of non-target elements were used.

3.2.1. Interferences from individual non-target elements

Standard solutions were prepared at four increasing levels (between 0 and maximum levels defined in Table 4) of each element (Na, Mg, K, Ca, Cu, Cr, V, Mn, Fe, Co, Ni, Zn, Ge, Br and Se) to create potential disturbing polyatomic interferences, and the response of the seven elements V, Cr, Fe, Co, Ni, As and Se was recorded. On the basis of the data collected during the first French Total Diet Study

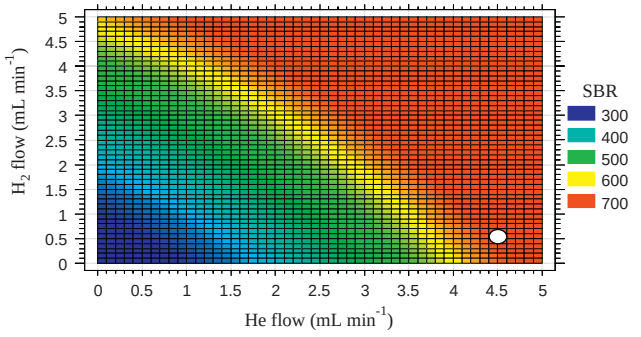

Fig. 2. Contour plot (2-D) showing the effects of the He flow and H_2 flow variables at fixed Hexapole bias and Quadrupole bias (−9.0 and −13.2 V, respectively) on the SBR response.

Table 4
Possible generated polyatomic species (estimated amounts in brackets in mg kg^{-1}) after spiking of each element at maximum range amount[a] (nebuliser flow = 0.90 mL min^{-1}).

Interferent	Detectable or Quantifiable polyatomic species							
	^{56}Fe CCT	^{59}Co	^{59}Co CCT	^{60}Ni	^{60}Ni CCT	^{75}As CCT	^{82}Se	^{80}Se CCT
Na	$^{23}Na^{16}O_2{}^1H^+$ (0.185)	–	–	–	–	–	–	–
Mg	$^{24}Mg^{16}O_2{}^+$ (0.641)	–	–	–	–	–	–	–
Ca	$^{40}Ca^{16}O^+$ (0.224)	$^{43}Ca^{16}O^+$, $^{42}Ca^{16}O^1H^+$ (0.021)	$^{43}Ca^{16}O^+$ (0.019)	$^{44}Ca^{16}O^+$, $^{43}Ca^{16}O^1H^+$ (0.381)	–	$^{43}Ca^{16}O_2{}^+$ (0.046)	–	–
Fe	–	–	–	–	–	$^{54}Fe^{18}O^1H^+$ (<LOQ)	–	–
Co	–	–	–	–	$^{59}Co^1H^+$ (0.170)	$^{59}Co^{16}O^+$ (<LOQ)	–	–
Ni	–	–	$^{58}Ni^1H^+$ (0.010)	–	–	$^{58}Ni^{16}O^1H^+$ (<LOQ)	–	–
Ge	–	–	–	–	–	$^{74}Ge^1H^+$ (0.019)	–	–
Br	–	–	–	–	–	–	$^{81}Br^1H^+$ (8.95)	$^{79}Br^1H^+$ (2.33)

[a] [Ge] = [Se] = 2 mg kg^{-1}, [Zn] = [Cu] = Ni] = [V] = [Cr] = [Co] = 20 mg kg^{-1}, [Mn] = 50 mg kg^{-1}, [Br] = [Fe] = 500 mg kg^{-1}, [Mg] = 3000 mg kg^{-1}, [Ca] = [Na] = [K] = 10,000 mg kg^{-1}.

[36] and the certified values of the commercially available CRMs, the upper levels for each element were determined as exceeding the maximum amounts that can be reasonably encountered in foodstuffs. Table 4 summarises the maximum amounts present at the different *m/z* and the possible identity of the polyatomic ions generated. The amounts of these interferences were calculated at the highest standard addition amounts of non-target elements, for a sample weight of 0.3 g and a final dilution volume of 50 mL. To facilitate the reading of the results presented in Table 4, if for example, 10,000 mg kg^{-1} of Ca was added without any iron to the solution, 0.224 mg kg^{-1} at *m/z* = 56 was detected in CCT conditions, probably due to the interference from $^{40}Ca^{16}O^+$. Neither ^{54}Fe and ^{75}As in standard mode, nor ^{51}V, ^{52}Cr in both modes, appear on the table since these isotopes were not disturbed. Similarly, the results of the spike for K, Cu, Cr, V, Mn, Zn and Se are not displayed since there was no signal effect on any of the seven elements. Among the identifiable first-order polyatomic interferences with the different isotopes used in standard mode, $^{43}Ca^{16}O^+$ for $^{59}Co^+$ was also present in CCT mode, but the amount of this interference remained very low. In addition, the polyatomic interference BrH^+ ($^{79}Br^1H^+$ and $^{81}Br^1H^+$ for ^{80}Se and ^{82}Se, respectively), was present in both modes. Note that the amount of this interference diminished by about four-fold, while its sensitivity increased by about 3.8-fold from standard to CCT mode, indicating that the overestimation of Se would be greater through standard mode analysis and that such interference was not significantly alleviated by the optimised CCT. Otherwise, it should be noted that the majority of polyatomic ions were identified in CCT mode whereas they were absent in standard mode, revealing the second-order nature of these interferences. Two types of second-order interferences were listed: oxygen- and hydrogen-based polyatomic ions. On the one hand, water vapour or molecular oxygen in the cell gas may have led to these interferences [37]. On the other hand, pressurisation of the collision cell with pure H_2 gas clearly contributed to the formation of the possible second-order interferences $^{58}Ni^1H^+$, $^{59}Co^1H^+$, and $^{79}Br^1H^+$. Furthermore, considering the value of the upper levels for the non-targeted elements, these interferences were insignificant in CCT mode, except for Na, Mg and Ca on ^{56}Fe, Co on ^{60}Ni and Br on ^{80}Se. As a consequence, an overestimation of ^{56}Fe amounts will occur when analysing e.g. salted meat, spinach or cocoa beverages and dairy products, containing respectively large amounts of Na, Mg and Ca (more than 1000, 500 and 5000 mg kg^{-1}, respectively). Nonetheless, this positive bias would not be significant regarding the large levels of Fe likely to be quantified in these matrices. Conversely, the determination of low amounts of ^{60}Ni in seafood products may be hampered since they can contain several mg kg^{-1} of Co. Finally, selenium quantification based on ^{80}Se cannot therefore be used directly for the analysis of real samples with the new potential interferences $^{79}BrH^+$ (Table 4). As defined in the literature [34,41], an appropriate correction equation for the signal at *m/z* = 80 taking into account bromine hydridation should be applied to remove this bias:

$$I_{80Se} = I_{80} - a \times I_{79Br} - I_{80Kr},$$

where *I*: intensity of selected mass; *a*: rate of hydridation of bromine (%).

By plotting the calibration graphs of the standard solution, the bromine hydridation rate was determined at 1.1%. Furthermore, the signal of Kr was inhibited by CCT mode. So, this correction equation was used systematically in CCT mode for the determination of ^{80}Se.

3.2.2. Interferences from a mixture of non-target elements

From the results of Table 4, the elements which were considered to have a spectroscopic influence on a particular target analyte were added together at their upper level on six standard solutions containing the seven elements of interest, ranging from 0 to 50 μg L^{-1}.

Table 5
Standard solution addition effect on signal of V, Cr, Fe, Co, Ni, As and Se in CCT mode (Neb flow = 0.90 mL min^{-1} and 0.76 mL min^{-1}).

	Mixture added	V	Cr	Fe	Co	Ni	As	Se
	I	1.37	1.20	NQ	1.02	1.04	1.34	1.20
	II	1.39	1.28	1.15	1.16	–	1.26	1.15
Slope ratio	III	1.12	1.11	1.09	–	1.10	1.09	1.07
Neb flow = 0.90 mL min^{-1}	IV	1.31	1.30	1.10	1.09	1.14	0.98	1.03
	V	1.30	1.20	–	1.16	–	1.25	1.15
	I	1.15	1.12	NQ	1.12	0.99	1.19	1.14
	II	1.14	1.13	1.13	1.14	–	1.17	1.08
Slope ratio	III	1.09	1.08	1.06	–	1.07	1.04	1.02
Neb flow = 0.76 mL min^{-1}	IV	1.10	1.08	1.07	1.08	1.06	0.92	0.95
	V	1.08	1.06	–	1.07	–	1.10	1.01

I: Na, Mg, Ca; II: Ca, Ni; III: Co; IV: Br; V: Ca, Fe, Co, Ni, Ge with [Mg] = 3000 mg kg^{-1}, [Ca] = [Na] = 10,000 mg kg^{-1}, [Ni] = [Co] = 20 mg kg^{-1}, [Br] = [Fe] = 500 mg kg^{-1}, [Ge] = 2 mg kg^{-1}.
NQ: Not quantified.

Table 5A presents the slope ratio corresponding to the addition of these mixtures (or individual additions in the case of Co and Br) of interfering elements (from I to V) at the upper level. Only an enhancement of the slope of more than 1.20 (20%) is consider significant (based on the intermediate precision $CV_R = 10\%$, $k = 2$, defined previously [14]). All the calibration curves have a satisfactory determination coefficient ($r^2 > 0.995$, based on a minimum of four data points), except for Fe with mixture I (Na, Mg, Ca). Indeed, the ^{56}Fe slope was strongly affected by the addition of mixture I and it was not possible to obtain reliable data. The addition of several of these mixtures (from I to V) led overall to an overestimation of the response of the different standards. It should be noted that the standard mode was more affected by these drastic conditions (data not shown). As an example, the addition of 20 mg kg^{-1} of Co (mixture III) induced a non significant overestimation of about 10% of the slope in CCT mode and between 15 and 56% in standard mode for the selected elements. This clearly also indicates the occurrence of non-spectroscopic interferences, as previously observed [42]. Until now, the mechanism involved has still not been completely elucidated. Fraser and Beauchemin proposed that it could result from the occurrence of an enhancement in the ion beam, when an easier ionic transmission of the target elements takes place [36]. Co, Ni and Fe (except for mixture I) were not disturbed whereas V, Cr, As and Se were significantly affected by several mixtures, as listed in Table 5A. ^{51}V and ^{52}Cr signals, which were not previously disturbed by spectroscopic interferences, were the most positively affected by all the mixtures (except the individual addition of Co to mixture III), since their respective slopes increased by a maximum of 39 and 30% after the addition of mixtures II (Ca, Ni) and IV (Br), respectively. The ^{75}As signal was enhanced by the presence of Ca, with a maximum increase in its slope of 34% (mixture I), which is equivalent to overestimating by 1.7 mg kg^{-1} a sample whose real concentration would be 5 mg kg^{-1}. This overestimation is greater than that observed in Table 4 when adding the overestimation due to the individual interfering elements at *m/z* 75 (about 0.065 mg kg^{-1} for Ca, Fe, Co, Ni and Ge), probably due to the occurrence of signal elimination or enhancement depending on the sample matrix composition [37]. ^{80}Se showed a significant increase in its slope (20%) only in mixture I and not in mixture IV (Br addition). However, it should be noted that although the Se slope remained constant, this was due to the effect of the correction equation on the BrH^+ interference. In fact, without correction, the influence of this spectroscopic interference is also significant and could lead to a significant overestimation on ^{80}Se, as shown in Table 4.

3.2.3. Effect of decreasing nebuliser flow

As previously published, the signal enhancement due to these interferences could be reduced by decreasing the nebuliser flow [26,43]. After having initially optimised the instrument's sensitivity at a maximum flow rate of 0.90 mL min^{-1}, the flow was diminished until the sensitivity was divided by a threshold factor of about 4 (checked by the ^{115}In signal). As listed in Table 5B the analysis at a low flow rate of 0.76 mL min^{-1} made it possible to reduce the positive bias of the target element slopes. The overestimation of the quantifiable amounts decreased for all the elements to a non-significant level. Consequently, the lowering of nebuliser flow was considered beneficial for significantly reducing non-spectroscopic interferences. Indeed, the nebuliser flow decrease led to higher plasma temperature allowing thus a higher yield of isotopes ionization and a lower matrix effect.

3.2.4. Influence of dilution and decreasing nebuliser flow on trueness

The literature also reports that non-spectroscopic effects could be reduced not only through decreasing the nebuliser flow but also by sample dilution before analysis [43]. Thus, on the basis of the optimised settings (He flow: 4.5 mL min^{-1}; H_2 flow: 0.5 mL min^{-1}; quadrupole bias: −9.0 V; hexapole bias: −13.2 V), five samples of the CRM IAEA 407 were digested in triplicate and subjected on one side to three-fold, five-fold and ten-fold dilutions. On the other side, the non-diluted extracts were analysed at four decreasing nebuliser flows, 0.90, 0.85, 0.80 and 0.76 mL min^{-1}. As displayed in Fig. 3a and b, decreasing the nebuliser flow or diluting the sample both led to improved trueness, especially As in particular. For the other elements, the best results within the confidence interval were observed for conditions D (0.76 mL min^{-1}) and F (five-fold dilution), excepted V with the best results obtained in condition C (0.80 mL min^{-1}). So, to assess the effect of decreasing nebuliser flows and dilution on sensitivity, the limits of quantification were estimated in conditions A to F according to the NF EN 13804 standard and were defined as six times the standard deviation of the average from the 21 different sample blanks quantified over several months after correction for sample weight (0.3 g) and dilution [30]. A five-fold dilution multiplied the LOQ by the same factor, whereas a reduction in nebuliser flow had a less negative impact on sensitivity (Table 6). Indeed, at the minimum nebuliser flow rate, the LOQs were multiplied by about one to three-fold.

Consequently, and despite the slightly less satisfying trueness, the reduction in the nebuliser flow limited the increase of LOQ compared to a five-fold dilution. Additionally, it had the advantage of treating all the samples without an additional dilution step. The method was thus validated by systematically applying the

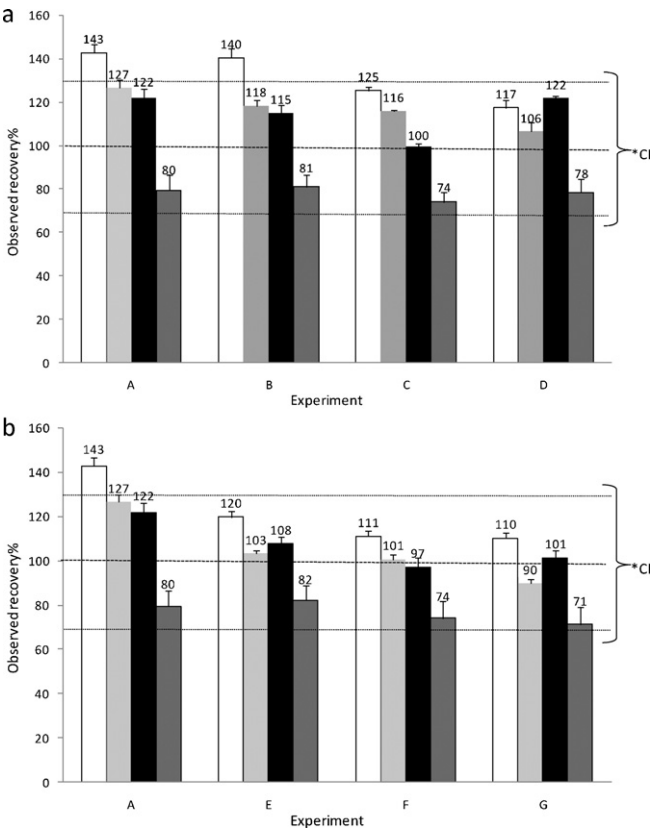

Fig. 3. (a) Observed recovery for As (white), Se (light grey), V (black) and Cr (grey) in CRM IAEA 407 ($n = 3$) at decreasing nebuliser flow values (A) 0.90, (B) 0.85, (C) 0.80 and (D) 0.76 mL min^{-1}. * $CI = M \pm [k \times ((CV_R \times M)/(100 \times \sqrt{n}))]$ with $k = 3$, $n = 1$ sample, $M = 100\%$ and CV_R arbitrarily set at 10%. (b) Observed recovery for As (white), Se (light grey), V (black) and Cr (grey) in CRM IAEA 407 ($n = 3$) at increasing dilution factors (A) 1, (E) 3, (F) 5 and (G) 10 at maximum nebuliser flow. * $CI = M \pm [k \times ((CV_R \times M)/(100 \times \sqrt{n}))]$ with $k = 3$, $n = 1$ sample, $M = 100\%$ and CV_R arbitrarily set at 10%.

Table 6
Influence of nebuliser flows and dilution factors on LOQ.

			LOQ (mg kg^{-1})						
			V	Cr	Fe	Co	Ni	As	Se
		0.90	0.003	0.018	0.187	0.004	0.085	0.006	0.011
	Nebuliser flow (mL min^{-1})	0.85	0.003	0.025	n/a	0.004	0.086	0.006	0.013
		0.80	0.003	0.025	n/a	0.004	0.191	0.006	0.016
CCT		**0.76**	**0.003**	**0.025**	**0.237**	**0.004**	**0.254**	**0.008**	**0.027**
		0	0.003	0.018	0.187	0.004	0.085	0.006	0.011
	Dilution factor	3	0.009	0.054	0.561	0.012	0.255	0.018	0.033
		5	0.015	0.090	n/a	0.020	0.425	0.030	0.055
		10	0.030	0.180	n/a	0.040	0.850	0.060	0.110
Standard[a]			*0.005*	*0.041*	*0.794*	*0.004*	*0.097*	*0.008*	*0.125*

n/a: not available;
[a] Neb flow = 0.90 mL min^{-1}.

nebuliser flow diminution approach after initial optimisation of the instrument's sensitivity at a high flow rate.

3.3. Method validation results

3.3.1. Range of linearity and LOQ

To carry out this study, six concentration levels ranging from 0 to 50 μg L^{-1} (0, 2, 5, 10, 20 and 50 μg L^{-1}) were prepared and analysed (n = 7). For all seven elements, the linear regression model was acceptable and no deviation from the regression model was observed in the defined range (data not shown). As described above, the LOQs were established for the target elements listed in bold in Table 6. In comparison, the LOQs measured in standard mode are displayed in italics. Globally, the optimised CCT mode remains the most sensitive in spite of the nebuliser flow decrease. Nevertheless, the LOQ of ^{60}Ni (0.254 mg kg^{-1}), which increased by about three-fold when the nebuliser flow was decreased from the highest to the lowest value, was significantly higher than the LOQ evaluated in standard mode (0.097 mg kg^{-1}).

3.3.2. Specificity

According to the NF V03-110 standard [31], to check the specificity of the method (lack of interferences), recoveries of spiked standard solutions in the defined calibration range were measured in several matrices after digestion. The amounts added were similar to those initially quantified in the different food samples. For each element, a graph was plotted using the amount added versus the amount recovered. The hypotheses of a slope different from 1 and an intercept different from 0 were evaluated using Student's t-test. Table 7 shows that t observed < t critical value for all elements (i.e. the slope and intercept of each regression line) was not equivalent to 1 and 0, respectively. As a consequence, the specificity of the method was considered acceptable.

3.3.3. Precision under repeatability and intermediate reproducibility conditions

The precision under repeatability (calculated as percentage coefficient of variation) CV_r was estimated by performing an analysis of p > 10 different samples (e.g. shrimp, scallop, ham, liver, hamburger, seeds, etc.) and n > 2 replicates [31]. For each analyte, $CV_r = (100 \times s_r/M)$ where M is the mean of observed values, and s_r^2 is the repeatability variance, was determined through the analysis of different samples at various levels. The Cochran test was performed in order to check the stability of the precision. The results demonstrated that the variance was homogeneous for the seven target analytes with max $(s)^2$ or log max $(s)^2$ < critical value, and the within-test variance showed acceptable repeatability CV_r varying from 4.8 to 9.2% (Table 8). In addition, the intermediate precision reproducibility was assessed by quantifying a CRM (TORT 2) in duplicate more than 10 times on different days over several months, with four different operators but with the same instrument: $CV_R = (100 \times s_R/M) = (100 \times \sqrt{s_r^2 + s_L^2}/M)$, where s_L^2 is the variance that measures sample variations and s_r^2 the repeatability variance [31]. The intermediate precision CV_R was in the range of 8.8–13.7% depending on the element (Table 9). This range of CV_R is very similar to those observed in standard mode conditions [14,44]. For practical reasons and for assessing the uncertainty measurement of the method, the CV_R was extended to 15% for all elements.

3.3.4. Trueness

The trueness of the method was evaluated by the same operator on TORT 2 (n = 6) according to the FD V03-115 standard [32]. The mean value of the six replicates should lie between the confidence interval (CI) determined from the certified value (M) of the CRM as:

$$CI = M \pm \left[k \times \frac{CV_R \times M}{100 \times \sqrt{n}} \right],$$

where k = 3 (p = 99%), n = 6 and CV_R = 15%.

Good agreement between the observed and certified values was found with the defined CI and with the CI of the CRM for V, Fe, Co and Se, but not for Cr whose value was slightly lower than the CI (Table 9). Furthermore, Table 10 displays the results obtained with the other CRMs analysed in CCT and standard modes (IAEA 407, NIST 1573a, BCR 278R, FAPAS R 761). The calculation of the Z-scores enables the magnitude and the sign of the bias to be characterised at the same time, i.e. over- (Z > 0) or under-estimation (Z < 0). The statistics of a normal distribution reveal that about 95%

Table 7
Results of specificity test.

	V	Cr	Fe	Co	Ni	As	Se
Slope (line of unity slope = 0)	1.076	0.958	0.933	0.979	1.005	1.099	0.938
Standard Deviation (s) of the slope	0.031	0.035	0.047	0.027	0.029	0.080	0.049
Intercept (line of unity intercept = 1)	0.149	0.478	1.315	0.121	-0.013	0.041	0.404
s of the intercept	0.303	0.371	1.100	0.275	0.277	0.806	0.470
Number of determinations	50	43	21	46	48	44	50
$T_{Critical\ value}$	2.682	2.701	2.861	2.692	2.687	2.698	2.682
$T_{observed}$ – Hypotheses test of slope ≠ 1	2.428	1.205	1.416	0.784	0.167	1.235	1.268
$T_{observed}$ – Hypotheses test of intercept ≠ 0	0.491	1.287	1.195	0.440	0.047	0.051	0.860

Table 8
Results of repeatability (precision under repeatability conditions) test (mg kg^{-1}).

	s_r[a]	s_r^2	CV_r mean (%)	Max $(s)^2$ or Log Max $(s)^2$	Cochran test (critical value = 0.6840)[b]
V	0.1264	0.0160	7.8	6.0744	0.1613
Cr	0.1070	0.0114	9.2	5.0503	0.1223
Fe	1.5353	2.3571	4.8	9.0155	0.3477
Co	0.0968	0.0094	5.4	9.2501	0.1561
Ni	0.1075	0.0116	8.0	5.9543	0.1295
As	0.3388	0.1148	6.5	0.5792	0.4587
Se	0.1404	0.0198	8.2	4.7297	0.1422

[a] 11 various samples at different levels in the defined linear range for the 8 elements and $n = 2$ measurement values.
[b] Critical value at the 1% significance level ($p = 11$; $n = 2$).

Table 9
Results of trueness and intermediate precision reproducibility.

	TORT 2	Mean (mg kg^{-1})	s (mg kg^{-1})	CV (%)	CI (mg kg^{-1})
V	Observed mean	1.79	0.03	1.5	
	Certified value	1.64	0.06	3.9	1.45–1.83[a]
	Reproducibility			10.2[b]	1.34–1.94[c]
Cr	Observed mean	0.56	0.02	4.2	
	Certified value	0.77	0.05	6.5	0.62–0.92[a]
	Reproducibility			13.7[b]	0.63–0.91[c]
Fe	Observed mean	98	1	1.0	
	Certified value	105	4	4.1	92–118[a]
	Reproducibility			8.b	86–124[c]
Co	Observed mean	0.48	0.00	1.0	
	Theoretical value	0.51	0.03	5.9	0.42–0.60[a]
	Reproducibility			11.5[b]	0.41–0.60[c]
Ni	Observed mean	2.12	0.03	1.2	
	Certified value	2.50	0.06	2.5	2.31–2.69[a]
	Reproducibility			12.3[b]	2.04–2.96[c]
As	Observed mean	24.2	0.5	1.9	
	Certified value	21.6	0.6	2.8	19.8–23.4[a]
	Reproducibility			11.8[b]	17.6–25.6[c]
Se	Observed mean	6.25	0.17	2.7	
	Certified value	5.63	0.23	4.1	4.96–6.30[a]
	Reproducibility			12.9[b]	4.60–6.66[c]

[a] Confidence interval of the CRM.
[b] CV_R = Intermediate precision coefficient of variation.
[c] $CI = M \pm [k \times ((CV_R \times M)/(100 \times \sqrt{n}))]$, where $k = 3$, $n = 6$, M = reference value and $CV_R = 15\%$.

Table 10
Compared CRM results (mg kg^{-1}) in CCT and standard modes.

Analyte	Reference material	Certified value[a]	CCT mode		Standard mode	
			Observed value	Z-score[b]	Observed value	Z-score[b]
V	TORT 2	1.64 ± 0.19	1.79	0.6	1.82	1.0
	IAEA 407	1.43 ± 0.09	1.35	−0.4	1.29	−1.1
	NIST 1573 a	0.835 ± 0.010	0.652	−1.9	0.590	−4.2
Cr	TORT 2	0.77 ± 0.15	0.56	−2.5	0.81	0.3
	IAEA 407	0.73 ± 0.06	0.56	−2.0	0.67	−0.6
	BCR 278R	0.78 ± 0.06	0.71	−0.7	0.91	1.0
	NIST 1573 a	1.99 ± 0.06	1.50	−2.2	1.46	−2.4
Fe	TORT 2	105 ± 13	98	−0.5	76	−2.5
	IAEA 407	146 ± 3	123	−1.2	86	−4.7
	NIST 1573 a	368 ± 7	318	−1.0	222	−4.4
Co	TORT2	0.51 ± 0.09	0.48	−0.4	0.46	−1.1
	IAEA 407	0.10 ± 0.01	0.08	−0.7	0.09	−1.1
	NIST 1573 a	0.57 ± 0.02	0.52	−0.6	0.48	−1.9
Ni	TORT 2	2.50 ± 0.19	2.12	−1.2	2.12	−1.2
	IAEA 407	0.60 ± 0.05	0.44	−2.4	1.07	2.9
	NIST 1573 a	1.59 ± 0.07	1.48	−0.5	2.33	2.1
As	TORT 2	21.6 ± 1.8	24.2	0.7	24.8	0.9
	IAEA 407	12.6 ± 0.3	14.0	0.7	13.3	0.4
	BCR 278R	6.07 ± 0.13	6.77	0.7	7.13	1.0
	NIST 1573 a	0.112 ± 0.004	0.182	2.6	0.699	5.6
	FAPAS R 761	0.054 ± 0.012	0.089	2.6	0.072	1.7
Se	TORT 2	5.63 ± 0.67	6.57	1.0	7.25	1.5
	IAEA 407	2.83 ± 0.13	2.77	−0.1	2.96	0.3
	BCR 278R	1.84 ± 0.10	1.79	−0.2	2.42	1.6
	NIST 1573 a	0.054 ± 0.003	0.069	1.4	2.11	6.5

[a] Uncertainty given at 95% confidence interval.
[b] Z-score $= (\overline{Xf} - \overline{Xc})/(S_R)$ where $\overline{Xc}$ is the certified value and S_R the standard deviation for the intermediate precision reproducibility ($n = 1$).

of data points will lie between a *Z*-score of −2 and +2; when the absolute value of *Z*-score was between 2 and 3, results were questionable. When the absolute value of *Z*-score was greater than or equal to 3, results were unacceptable.

The results obtained in CCT mode were generally satisfactory and more accurate since the *Z*-scores were smaller in absolute value than in standard mode (Table 10). Furthermore, the unacceptable *Z*-scores ($|Z| > 3$) obtained in standard mode (V, As, Fe, Se in NIST 1573a and Fe in IAEA 407) were reduced in CCT mode to acceptable or at least questionable *Z*-scores. It should be noted that the correction equation of Br was very useful for the determination of ^{80}Se, notably with NIST 1573a. The *Z*-score of As in NIST 1573a was reduced from 5.6 in standard mode to 2.6, suggesting persistence of the interferences in spite of the very significant improvement in trueness in CCT mode. It is probable that the trueness could not be improved further, due to a persistent spectroscopic interference such as that from the polyatomic ions $^{40}Ca^{35}Cl^{+}$ which were not completely eliminated ([Ca] = 50,500 mg kg^{-1}, [Cl] = 6600 mg kg^{-1}) or due to non-spectroscopic interferences likely to persist in such rich matrices ([Ca] = 50,500 mg kg^{-1}, [Mg] = 12,000 mg kg^{-1}) as discussed in Section 3.2.2.

Finally, the *Z*-scores for Cr (TORT 2, IAEA 407) and As (R 761) in CCT mode were above the ones in standard mode, but remained acceptable or ($|Z| < 3$). For Cr, the explanation of the underestimations observed on these CRMs in CCT mode remains unknown. However, the degradation of the *Z*-score of As in CCT mode was expected ($Z = 2.6$ instead of 1.7 in standard mode), due to both the persistence and the newly in-cell formed polyatomic ion $^{40}Ca^{35}Cl^{+}$ in such a rich matrix (2190 mg Ca kg^{-1} estimated). This demonstrates the limits of the CCT method, whatever the conditions used to accurately quantify low contents of As in a matrix containing high Ca level such as milk and milk products.

4. Conclusion

The experimental design methodology enabled the optimum CCT parameters to be set in order to drastically reduce first-order spectroscopic interferences observed by ICP-MS detection. Nevertheless, it was demonstrated that second-order spectroscopic interferences may form and persist since the optimised quadrupole and hexapole voltages did not enable kinetic energy discrimination. Indeed, even though the overall interferences were considered negligible, the in-cell formation of $^{79}Br^{1}H$ may induce a significant positive bias on the ^{80}Se signal. That is why the H_2 flow was set as low as possible at the conclusion of the optimisation process with the use of an appropriate correction equation. On the other hand, non-spectroscopic interferences, which may occur in rich food samples, could not be influenced by CCT but were successfully attenuated by decreasing nebuliser flow with acceptable LOQ, for some particular matrices, an overestimation might occur. In addition, CCT mode showed better recoveries overall for CRM analysis compared to standard mode, except for Cr which was often underestimated. Finally, the method validation process showed satisfactory results for all seven elements in the most common food samples.

References

[1] World Health Organization. Trace Elements in human nutrition and health. ISBN: 92 4 156173 4 (NLM Classification: QU 130), 1996.
[2] R. Kroes, D. Muller, J. Lambe, M.R.H. Lowik, J. van Klaveren, J. Kleiner, R. Massey, S. Mayer, I. Urieta, P. Verger, A. Visconti, Food Chem. Toxicol. 40 (2002) 327–385.
[3] S.L.C. Ferreira, W.N.L. dos Santos, V.A. Lemos, Anal. Chim. Acta 445 (2001) 145–151.
[4] G. Doner, A. Ege, Anal. Chim. Acta 520 (2004) 217–222.
[5] M.C. Yebra, S. Cancela, R.M. Cespon, Food Chem. 108 (2008) 774–778.
[6] M. Ghaedi, A. Shokrollahi, A.H. Kianfar, A.S. Mirsadeghi, A. Pourfarokhi, M. Soylak, J. Hazard. Mater. 154 (2008) 128–134.
[7] M.S. Bratakos, E.S. Lazos, S.M. Bratakos, Sci. Total Environ. 290 (2002) 47–58.
[8] A. Paiva Oliveira, J. Anchieta Gomes Neto, J. Araujo Nobrega, P. Rogerio Miranda Correia, P. Vitoriano Oliveira, Food Chem. 93 (2005) 355–360.
[9] P. Viñas, M. Pardo-Martınez, M. Hernández-Córdoba, Anal. Chim. Acta 412 (2000) 121–130.
[10] C. Cabrera, F. Lloris, R. Gimenez, M. Olalla, M.C. Lopez, Sci. Total Environ. 308 (2003) 1–14.
[11] S.P. Dolan, S.G. Capar, J. Food Compos. Anal. 15 (2002) 593–615.
[12] C. Peña-Farfal, A. Moreda-Piñeiro, A. Bermejo-Barrera, P. Bermejo-Barrera, H. Pinochet-Cancino, I. de Gregori-Henrıquez, Talanta 64 (2004) 671–681.
[13] A. Ikema, A. Nwankwoalab, S. Odueyungboa, K. Nyavora, N. Egiebor, Food Chem. 77 (2002) 439–447.
[14] L. Noël, V. Dufailly, N. Lemahieu, C. Vastel, T. Guerin, J. AOAC Int. 88 (2005) 1811–1821.
[15] L. Noël, J.C. Leblanc, T. Guérin, Food Addit. Contam. 20 (2003) 44–56.
[16] R.M. Barnes, Anal. Chim. Acta 283 (1993) 115–130.
[17] E.P. Nardi, F.S. Evangelista, L. Tormen, T.D. Saint'Pierre, A.J. Curtius, S.S. de Souza, F. Barbosa Jr., Food Chem. 112 (2009) 727–732.
[18] M. Lamand, J-C. Tressol, J. Ireland-Ripert, J.C. Favier, M. Feinberg, Répertoire général des aliments T 4. Table de composition minérale, INRA, Paris, France, 1996, pp. 1–222.
[19] S.D. Tanner, V.I. Baranov, D.R. Bandura, Spectrochim. Acta B 57 (2002) 1361–1452.
[20] Y.L. Chang, S.J. Jiang, J. Anal. Atom. Spectrom. 16 (2001) 1434–1438.
[21] K.L. Chen, S.J. Jiang, Anal. Chim. Acta 470 (2002) 223–228.
[22] V. Dufailly, L. Noël, T. Guérin, Anal. Chim. Acta 565 (2006) 214–221.
[23] M. Grotti, R. Frache, J. Anal. Atom. Spectrom. 22 (2007) 1481–1487.
[24] W.J. McShane, R.S. Pappas, D. Paschal, J. Anal. Atom. Spectrom. 22 (2007) 630–635.
[25] R.Y. Wang, Y.L. Hsu, L.F. Chang, S.J. Jiang, Anal. Chim. Acta 590 (2007) 239–244.
[26] V. Dufailly, L. Noël, T. Guérin, Anal. Chim. Acta 611 (2008) 134–142.
[27] A.J. Bednar, Talanta 78 (2009) 453–457.
[28] S. D'Ilio, F. Petrucci, M. D'Amato, M. Di Gregorio, O. Senofonte, N. Violante, Anal. Chim. Acta 624 (2008) 59–67.
[29] A.J. Bueno Cotta, J. Enzweiler, J. Anal. Atom. Spectrom. 24 (2009) 1406–1413.
[30] Agence Française de Normalisation, NF EN 13804 Standard, AFNOR, Saint-Denis, France, 2002.
[31] Agence Française de Normalisation, NF V03-110 Standard, AFNOR, Saint-Denis, France, 1998.
[32] Agence Française de Normalisation, FD EN V03-115 Standard, AFNOR, Saint-Denis, France, 1996.
[33] G.E.P. Box, D.W. Behnken, Technometrics 2 (1960) 455–475.
[34] L. Hinojosa Reyes, J.M. Marchante Gayon, J.I. Garcia Alonso, A. Sanz-Medel, J. Anal. Atom. Spectrom. 18 (2003) 11–16.
[35] M.M. Fraser, D. Beauchemin, Spectrochim. Acta B 55 (2000) 1705–1731.
[36] J.C. Leblanc, T. Guérin, L. Noel, G. Calamassi-Tran, J.L. Volatier, P. Verger, Food Addit. Contam. 22 (2005) 624–641.
[37] B. Hattendorf, D. Gunther, J. Anal. Atom. Spectrom. 19 (2004) 600–606.
[38] M. Niemelä, P. Perämäki, H. Kola, J. Piispanen, Anal. Chim. Acta 493 (2003) 3–12.
[39] C.P. Ingle, P.K. Appelblad, M.A. Dexter, H.J. Reid, B.L. Sharp, J. Anal. Atom. Spectrom. 16 (2001) 1076–1084.
[40] S. Mazan, N. Gilon, G. Cretier, J. Anal. Atom. Spectrom. 17 (2002) 366–370.
[41] J. Darrouzes, M. Bueno, G. Lespes, M. Potin-Gautier, J. Anal. Atom. Spectrom. 20 (2005) 88–94.
[42] G.R. Gillson, D.J. Douglas, J.E. Fulford, K.W. Halligan, S.D. Tanner, Anal. Chem. 60 (1988) 1472–1474.
[43] M.A. Vaughan, G. Horlick, Appl. Spectrosc. 40 (1986) 427–573.
[44] S. Millour, L. Noël, A. Kadar, R. Chekri, C. Vastel, T. Guérin, J. Food Compos. Anal. 24 (2011) 111–120.